Effective Darcy-scale contact angles in porous media imbibing solutions of various surface tensions

Noam Weisbrod,[1] Thomas McGinnis,[2] Mark L. Rockhold,[3] Michael R. Niemet,[4] and John S. Selker[2]

Received 29 February 2008; revised 7 June 2009; accepted 22 June 2009; published 17 October 2009.

[1] Surface tensions of high-salinity solutions are significantly different from those of pure water. Our objective was to develop and test a methodology to determine whether these surface tension effects predictably alter imbibition into dry and moist porous media. Static and dynamic experiments were performed using four grades of quartz sand to determine the effects of solution salinity on imbibition. Results were quantified as apparent contact angles between the sand and three solutions (pure water, 5 molal $NaNO_3$, and n-hexane). Contact angles determined using a static method in initially air dried sand ranged from 23° to 31°, with the same values found for both water and the $NaNO_3$ solution. Effective contact angles determined for the air-dried sand using a dynamic method based on a modified version of the Green and Ampt model were about twice those found using the static method, averaging 45° and 62° for water and the $NaNO_3$ solution, respectively. In prewetted sands, the dynamic imbibition data yielded apparent contact angles of 2° and 21° for water and the $NaNO_3$ solution, respectively, with the latter value comparing well to a predicted value of 25° for the $NaNO_3$ solution solely on the basis of surface tension contrast. The results of this study indicate that on the Darcy scale, saline solutions appear to follow the relationship of nonzero contact angles with other miscible fluids of different surface tensions used to prewet the sand grains, in agreement with the macroscale infiltration results of Weisbrod et al. (2004).

Citation: Weisbrod, N., T. McGinnis, M. L. Rockhold, M. R. Niemet, and J. S. Selker (2009), Effective Darcy-scale contact angles in porous media imbibing solutions of various surface tensions, *Water Resour. Res.*, *45*, W00D39, doi:10.1029/2008WR006957.

1. Introduction

[2] Interfacial free energies (surface tensions) control the spontaneous imbibition of liquids into porous media [*Blake*, 1993]. Surface wetting has been reported to be a time-dependent process that is inhibited by physical and chemical surface irregularities [*Meyers*, 1991]. Viewed under a microscope [e.g., *Selker and Schroth*, 1998], the wetting front advances as a heterogeneous ensemble, with some areas wetting aggressively (0° contact angle), and others exhibiting hydrophobic behavior (>90° contact angle). We will refer to these locally observable contact angles as microscale contact angles (MCAs). Because of the wide industrial and natural occurrence, significant amount of work was done at the microscale to explore the infiltration of liquid droplets into porous media [e.g., *Clarke et al.*, 2002; *Daniel and Berg.*, 2006; *Denesuk et al.*, 1993; *Holman et al.*, 2002; *Hilpert and Ben-David*, 2009; *Zadrazil et al.*, 2006]. On the Darcy scale (defined here as a representative elementary volume containing thousands of grains), the net result of these complex processes can be represented by a single effective contact angle, which we will refer to as a Darcy-scale contact angle (DCA).

[3] The MCA may be geometrically defined as the angle formed by the intersection of two planes tangent to the liquid and solid surfaces at the point of contact between the two phases and a third, surrounding phase (typically gas). The point of contact among the three phases is commonly referred to as the three-phase contact point (Figure 1) or the wetting point [*Meyers*, 1991]. A liquid with a contact angle of less than 90° (such as pure water on clean glass) will cause spontaneous wetting or infiltration of a liquid into a porous medium such as sand.

[4] Although the idealized conceptual model depicted in Figure 1 is useful for visualization, real porous media are much more complex. Nevertheless, this conceptual model provides a conceptual framework for computing DCAs. Such computed DCAs represent larger-scale manifestations of physical-chemical processes occurring on much smaller scales that are not accessible to direct observation and measurement in real porous media.

[5] Obtaining the relationship between the contact angle, surface tension, and resulting capillary pressure for an idealized contact such as that depicted in Figure 1 is straightforward. Balancing forces in the horizontal direction at the contact point yields

$$\sum F = 0 = F_{sl} - F_{sg} + F_{\mathrm{lg}} \cos\gamma \qquad (1)$$

[1]Department of Environmental Hydrology and Microbiology, Ben-Gurion University of the Negev, Ben-Gurion, Israel.
[2]Department of Biological and Ecological Engineering, Oregon State University, Corvallis, Oregon, USA.
[3]Pacific Northwest National Laboratory, Richland, Washington, USA.
[4]CH2M HILL, Corvallis, Oregon, USA.

Copyright 2009 by the American Geophysical Union.
0043-1397/09/2008WR006957

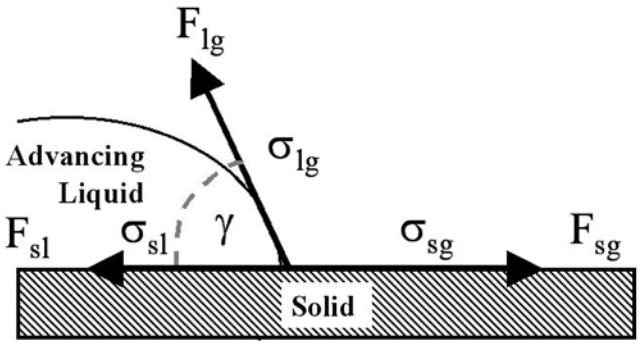

Figure 1. Three-phase line of contact between forces. Here F_{sg} is the solid-gas surface force per unit length, F_{lg} is the liquid-gas surface force, F_{sl} is the solid-liquid surface force, σ_{sg} is the relative surface tension between the solid and the gas, σ_{lg} is the relative surface tension between the liquid and the gas, and σ_{sl} is the relative surface tension between the solid and the liquid. The γ term denotes the contact angle.

where F_{sg} is the solid-gas surface force per unit length, F_{sl} is the solid-liquid surface force, F_{lg} is the liquid-gas surface force, and γ is the contact angle. When expressed on a per-unit-length basis, equation (1) may be written in terms of the relative surface tensions in the form of Young's equation:

$$\sigma_{sg} = \sigma_{sl} + \sigma_{\mathrm{lg}} \cos\gamma \tag{2}$$

where σ_{sg} is the solid-gas interfacial tension, σ_{sl} is the solid-liquid interfacial tension and σ_{lg} is the liquid-gas interfacial tension. Rearranging equation (2) to solve for the contact angle yields

$$\gamma = \cos^{-1}\left(\frac{\sigma_{sg} - \sigma_{sl}}{\sigma_{\mathrm{lg}}}\right) \tag{3}$$

[6] The well-known Young-Laplace equation relates the effective pore radius, r, of the porous media to the contact angle and capillary pressure, P_c,

$$P_c = \frac{2\sigma_{\mathrm{lg}} \cos\gamma}{r} \tag{4}$$

Throughout our analysis and experiments we assume that the nonwetting phase (air) is in free communication with the atmosphere and pressures are represented as gauge values in units of head.

[7] Wetting is a dynamic, rate-dependent process. Recognizing these temporal effects, *Meyers* [1991] refers to the contact angle of a moving wetting front as a dynamic contact angle. A static method is one in which the processes involved with imbibition are deemed to have stabilized or come to equilibrium, before the contact angle is calculated. However, in many practical applications, the wetting phenomena of interest involve moving wetting fronts [*Meyers*, 1991; *Siebold et al.*, 2000]. *Weisbrod et al.* [2002] postulated that a nonzero dynamic contact angle may have given rise to the fingering behavior observed in their experiments during imbibition of saline solutions into water-wetted sands.

[8] Our objective was to develop and test a methodology that could determine whether these surface tension effects predictably alter imbibition into dry and moist porous media in a Darcy-scale. We sought to determine if nonzero apparent DCAs develop when saline solutions imbibe into initially water-wetted silica sand, as suggested by *Weisbrod et al.* [2004]. To achieve this objective, it was necessary to develop a novel analytical method of interpreting dynamic imbibition data.

2. Materials and Methods

2.1. Experimental Setup

[9] Two capillary rise methods, static and dynamic, were used. The basic experimental system consisted of 20-cm long, 4.5-cm inside diameter (4.76-cm outside diameter) acrylic tubes packed with sand. For the dynamic experiments, the lower end of these columns was covered with a double layer of cheesecloth, while for the static experiments, a 0.0254-mm (500-mesh) stainless steel screen was used. The cheesecloth allowed for more rapid initial imbibition, but columns fitted with the stainless steel screen were more stable over longer experimental periods (Figure 2). The porous media used in the experiments were commercial silica sands (Accusand®, Unimin, Le Sueur, MN) of 40/50, 30/40, 20/30 and 12/20 grades [*Schroth et al.*, 1996]. Prior to use, the sand was rinsed 8–10 times with distilled water, until no turbidity was observed in the supernatant. The rinsed sand was then oven dried at 50°C for 48 h.

[10] The three infiltrating solutions employed were (solution A) 5 molal $NaNO_3$ solution; (solution B) distilled, deionized water (NANOpure 04751, Barnstead International, Dubuque, Iowa); and (solution C) n-hexane. Solution A was selected to simulate the >5 M Na concentration in the waste solutions leaked from Hanford Tanks [*Grand Junction Projects Office*, 1996] employed by *Weisbrod et al.* [2002, 2003, and 2004] (Table 1).

2.2. Experimental Procedure

[11] The columns were dry packed by continuous pouring into a fill tube which contained a series of screens to randomize the trajectory of the falling sand grains. Next, the packed columns were weighed. The packing method resulted in very homogeneous packs with porosities of 0.33 ± 0.02. In all of the experiments, the columns were vertically oriented. The temperature in the laboratory was kept at 22 ± 3°C throughout the duration of the experiments.

[12] In the static experiments, a sand-filled column was attached to a ring stand on a balance. The liquid of interest was poured into a beaker, placed on a small scissor jack, and slowly raised until the surface of the liquid just touched the bottom surface of the sand column. Plastic wrap was used to cover the mouth of the beaker and to seal the air space between the top of the beaker and the column to minimize evaporation. The tops of the columns were also covered with small cardboard covers to minimize evaporation, while allowing air to freely escape the columns during imbibition. The height of capillary rise was measured with a ruler every 2 h after the test was started. Final rise was determined when the wetting front had been stable for 6 h (typically after 24 h).

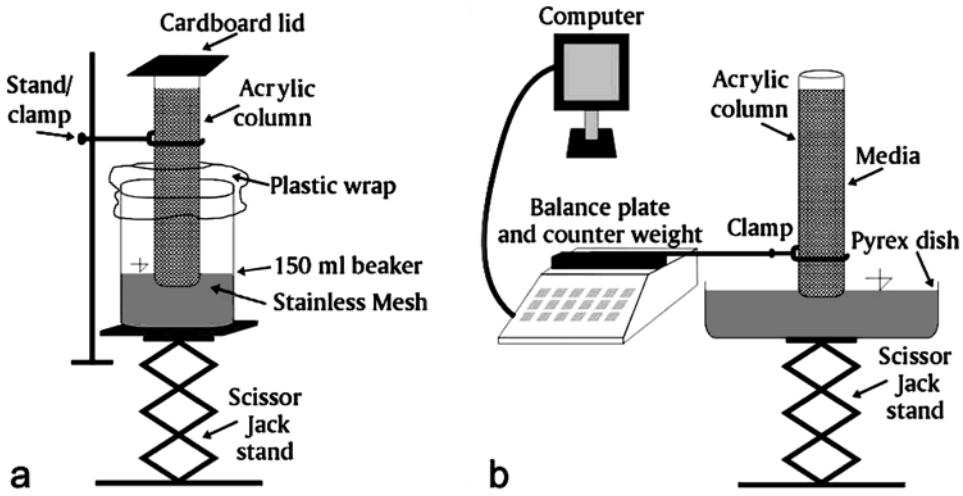

Figure 2. Schematics of the (a) static and (b) dynamic experimental setups.

Because the media used are essentially monodisperse, the position of the wetting front was fairly easily delineated. However, the apparent height of the rise was calculated from the volume and porosity of the sand-packed columns and the mass of imbibed solution, after correction for the mass contained in the retaining screen or cheesecloth, assuming fully liquid-saturated conditions behind the wetting front. Although a wetting front position could be clearly seen in most cases, if we measured the height of capillary rise using a ruler on the side of the column, and then used equation (6) with the measured masses and densities of imbibed liquids to calculate apparent liquid contents, we would not necessarily obtain values that were equivalent to the independently determined values of porosity. This was presumably due to inexact measurement of the height of capillary rise itself (e.g., from a somewhat diffuse rather than a sharp wetting front), and/or to entrapped air. It is well known that the porosity in the immediate vicinity of the wall of a sand-packed column or flow cell is greater than it is elsewhere, and can result in somewhat lower capillary rise and lower liquid saturations immediately adjacent to the walls relative to other areas during an imbibition experiment. Hence what seems like a simple direct observation may not result in an accurate measurement of the effective value of the parameter of interest. Since we were able to measure all of the other variables in equation (6) independently, and we could only use the apparent height in the dynamic tests, we chose to calculate the apparent height of capillary rise from the other measurements. Thirty-six experiments (three repetitions for each of three solutions and four sand grades) were performed.

[13] In the dynamic method, a pan (20 × 15 cm Pyrex® baking dish) of liquid on a scissor jack was raised until it just touched the bottom of the sand column. An electronic balance (5 kg Setra®) measured the mass of liquid imbibed into the columns and was automatically recorded every 3 s during imbibition. After quasi-static conditions had been reached, the pan was lowered until the meniscus broke and the experiment was terminated.

[14] The columns for testing the prewetted sand were prepared in the same way as for the dry sand experiments. The three columns were placed upright on top of a stainless steel mesh grating in a large bucket. The bucket was slowly filled with NANOpure® water to within 3.0 cm of the top of the columns. The columns were allowed to sit for 2 h to ensure complete saturation. Then they were removed from the water bath, allowed to drain freely overnight, and reweighed. The drained columns were then placed in a 40-cm-tall pressure extractor (model 1400 Soil Moisture Equipment, Inc., Santa Barbara, California) fitted with a 1 bar porous ceramic plate, and held at 0.2 bar for 12 h to drain the columns to residual water content.

2.3. Data Analysis

2.3.1. Static Tests

[15] The water pressure and gravitational potential acting on a porous medium are assumed to be in equilibrium when conditions are static. This state is represented by

$$h_s = \frac{2\sigma_{lg}\cos\gamma}{\rho_l g r} \tag{5}$$

where ρ_l is the liquid density, g the gravitational acceleration, h_s the height of rise of the liquid, and the subscript s is used here to denote a static condition. For the static method, a sharp wetting front and constant liquid content in the wetted volume were assumed. The capillary rise was calculated as

$$h_s = \frac{m_l}{\theta\pi\rho_l R_c^2} \tag{6}$$

where R_c is the radius of the column, and θ is the volumetric liquid content ($m^3\ m^{-3}$) of the wetted media (bounded by the

Table 1. Solution Properties[a]

Solution	Density (g/cm^3)	Viscosity (cP)	Surface Tension (mN/m)
n-hexane	0.659	0.314	18.4
5 molal $NaNO_3$	1.247	1.314	80.5
Pure water	0.992	1.001	72.8

[a]From *Weisbrod et al.* [2002].

Table 2. Fitted Values of K_{FS}, and θ_{FS} and Other Fixed Hydraulic Parameters

	40/50	30/40	20/30	12/20
K_{FS}[a] (cm/s)	0.043	0.071	0.107	0.102
K_S[b] (cm/s)	0.065	0.115	0.228	0.476
λ[c]	6.17	6.91	5.57	3.94
η[d]	3.324	3.289	3.359	3.508
θ_S[e] (cm^3/cm^3)	0.337	0.328	0.330	0.324
θ_0[c] (cm^3/cm^3)	0.020	0.018	0.016	0.012
θ_{fs}[f] (cm^3/cm^3)	0.300	0.286	0.267	0.211

[a]As fitted by the modified Green and Ampt solution.
[b]As measured using the falling head method.
[c]As reported by *Schroth et al.* [1996].
[d]As calculated from *Brooks and Corey* [1964] model.
[e]Average value based on the porosity of three packed columns per each of the four sand grades as prepared for the experiments.
[f]Degree of saturation θ_{fs} for K_{FS} fitted by the modified Green and Ampt solution.

porosity, n) and where m_l and ρ_l are the mass and density, respectively, of the imbibed liquid.

[16] To estimate r in equation (5), we used the low surface tension (σ_{lg} = 18.4 mN/m) n-hexane for which a contact angle (MCA) of 0° may be reasonably assumed [*Bachmann et al.*, 2003]. The value of r obtained for each grade of sand using n-hexane was assumed to be a constant characteristic of the porous medium. These values of r were used with equation (5) to compute DCA for imbibition with other less wetting liquids.

2.3.2. Dynamic Tests

[17] It has been widely observed that dynamic and static DCAs may not be equal, and thus we developed a method to estimate the DCA for a dynamic wetting process. A one-dimensional implementation of the analytical infiltration model developed by *Green and Ampt* [1911] provides a useful framework for the characterization of imbibition driven by capillary wetting in dynamic experiments [*Selker et al.*, 1999]. A basic assumption of the Green and Ampt model is that the wetting front is "sharp," which is consistent with the early character of upward imbibition in sandy soils, when $h \ll 2\sigma/\rho g$. A Green and Ampt–type model for vertical upward imbibition may be written as [e.g., *Malik et al.*, 1984; *McBride et al.*, 1992]

$$\frac{dh_d}{dt} = \frac{K_S}{n}\left[\frac{h_f - h_d}{h}\right] \tag{7}$$

where h_d is the capillary rise (with subscript d used to denote a dynamic condition), t is elapsed time, K_s is the saturated hydraulic conductivity, h_f is the pressure potential at the wetting front interface. Rearranging equation (7), substituting K_{FS} for K_s and θ_{FS} for n, and solving for t yields

$$t = \frac{\theta_{FS}}{K_{FS}}\left\{-h_d - h_f\left[\ln\left(\frac{h_f - h_d}{h_f}\right)\right]\right\} + t_0 \tag{8}$$

where t_0 is the constant of integration representing the apparent initial time of imbibition. Note that the terms K_s and n in equation (7) have been replaced with K_{FS} and θ_{FS} in equation (8) to indicate that the effective hydraulic conductivity and water content at the wetting front may not actually be the true saturated values because of nonuniform wetting and air entrapment during the imbibition process. The apparent or adjusted value of t in equation (8) was initially calculated by optimizing three parameters, t_0, K_{FS}, and h_f, using the solver add-in in Microsoft Excel. The parameter t_0 accounts for the very slight time lag during surface wetting that is observed after the imbibing solutions are initially brought into contact with the mesh at the bottom of the columns, but before actual imbibition into the sand occurs. The value t_0 also accounts for any delay between the time the data-logging program was started and the time the pan of liquid first touched the column, as well as any delay in reporting changes in mass due to stabilization of the electronics of the scale. The height of capillary rise, h_d, was calculated from the mass data using equation (6) (with h_d used in place of h_s).

[18] The fitted values of K_{FS} were always significantly smaller than the measured values of K_s obtained from saturated column experiments using a constant-head method [e.g., *Schroth et al.*, 1996]. This suggests, as has been widely reported, that behind the wetting front, the porous media was less than fully saturated. Therefore, after the initial parameter estimates were obtained, a secondary iteration process was used to update the values of θ_{FS} and corresponding values of K_{FS} used in equation (8) on the basis of *Brooks and Corey*'s [1964] water retention characteristics and *Burdine*'s [1953] relative permeability model

$$K_{FS} = K_S\left(\frac{\theta_{FS} - \theta_0}{n - \theta_0}\right)^{\eta} \quad \text{for} \quad h < h_f \tag{9}$$

where $\left[\eta = \frac{2}{\lambda} + 3\right]$, and λ is a pore interaction term, estimated from independent estimates of the water retention characteristics (primary drainage) of the porous media. Since we only seek a relationship between water content and hydraulic conductivity, the value of λ obtained in an independent drainage experiment is valid for the relationship between θ_{FS} and K_{FS}, regardless of whether this water

Table 3. K_S Determined Using the Falling Head Method Versus Fitted K_{FS} Determined by the Dynamic Method[a]

Sand	Solution	K_S Measured[b] (cm/s)	K_{FS} Fitted[c] (cm/s)	Ratio
40/50	n-hexane	0.065	0.028	2.40
	pure water	0.065	0.044	1.49
	$NaNO_3$	0.065	0.032	2.02
30/40	n-hexane	0.116	0.032	3.63
	pure water	0.116	0.072	1.62
	$NaNO_3$	0.116	0.050	2.35
20/30	n-hexane	0.230	0.030	7.78
	pure water	0.230	0.108	2.12
	$NaNO_3$	0.230	0.078	2.95
12/20	n-hexane	0.480	0.024	20.65
	pure water	0.480	0.103	4.64
	$NaNO_3$	0.480	0.122	3.95

[a]Each value is the mean of three repetitions.
[b]As measured using the falling head method [*Klute and Dirksen*, 1986].
[c]As fitted using the Green and Ampt model. Mean of three repetitions with acceptable standard deviation range of 0.002–0.039.

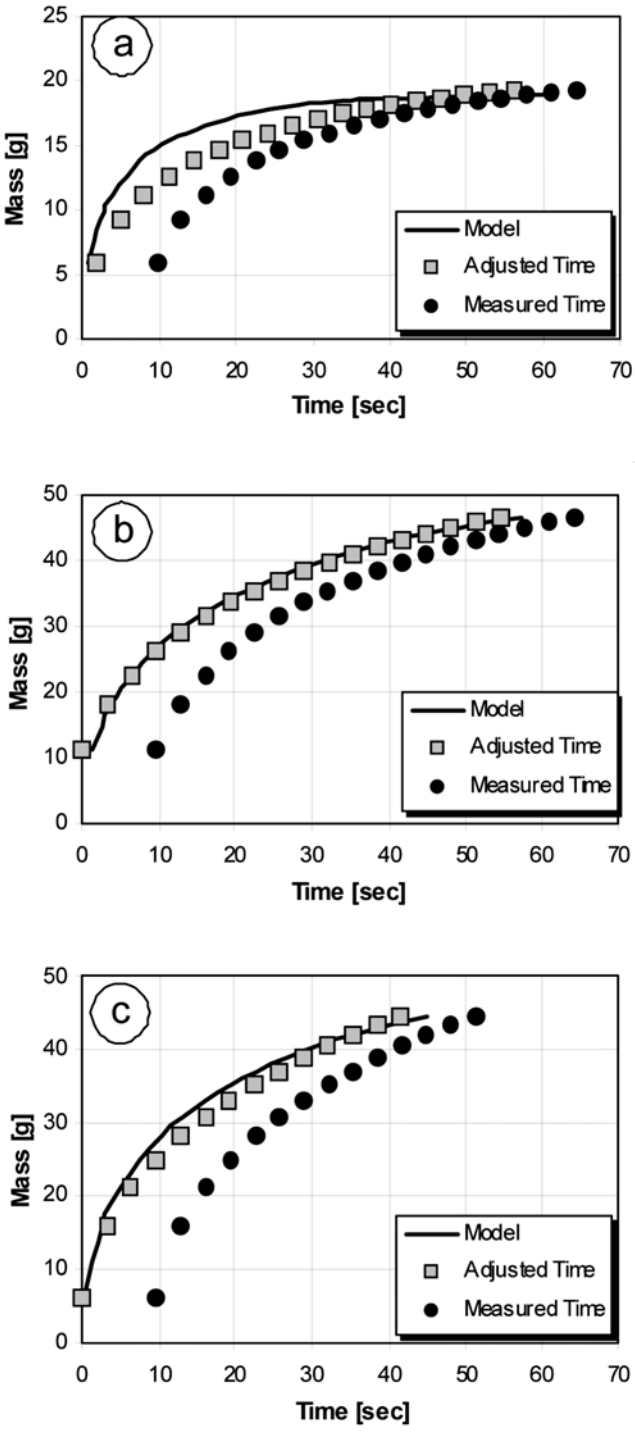

Figure 3. Imbibition of (a) n-hexane, (b) pure water, and (c) salt (5 molal $NaNO_3$) solution into air-dry 40/50 grade sand. Measured falling head K_S values are used in the Green and Ampt model, requiring the model to optimize only h_f and t_0.

content was achieved via wetting or draining. Equation (9) may be expressed in terms of θ as

$$\theta_{FS} = \left[(n - \theta_0) \left(\frac{K(\theta_{FS})}{K_S} \right)^{\frac{1}{\eta}} \right] + \theta_0 \qquad (10)$$

where $K(\theta_{FS})$ ($= K_{FS}$) represents the hydraulic conductivity at a given water content θ, θ_0 is the residual or non-reducible water content of the soil, n is the saturated water content (or porosity). Porosity was calculated from the mass and volume of the sand-packed columns (Table 2). Residual water content θ_0 and pore interaction parameter λ from *Schroth et al.* [1996] were used to represent the prewetted sands, while residual water contents were taken to be zero

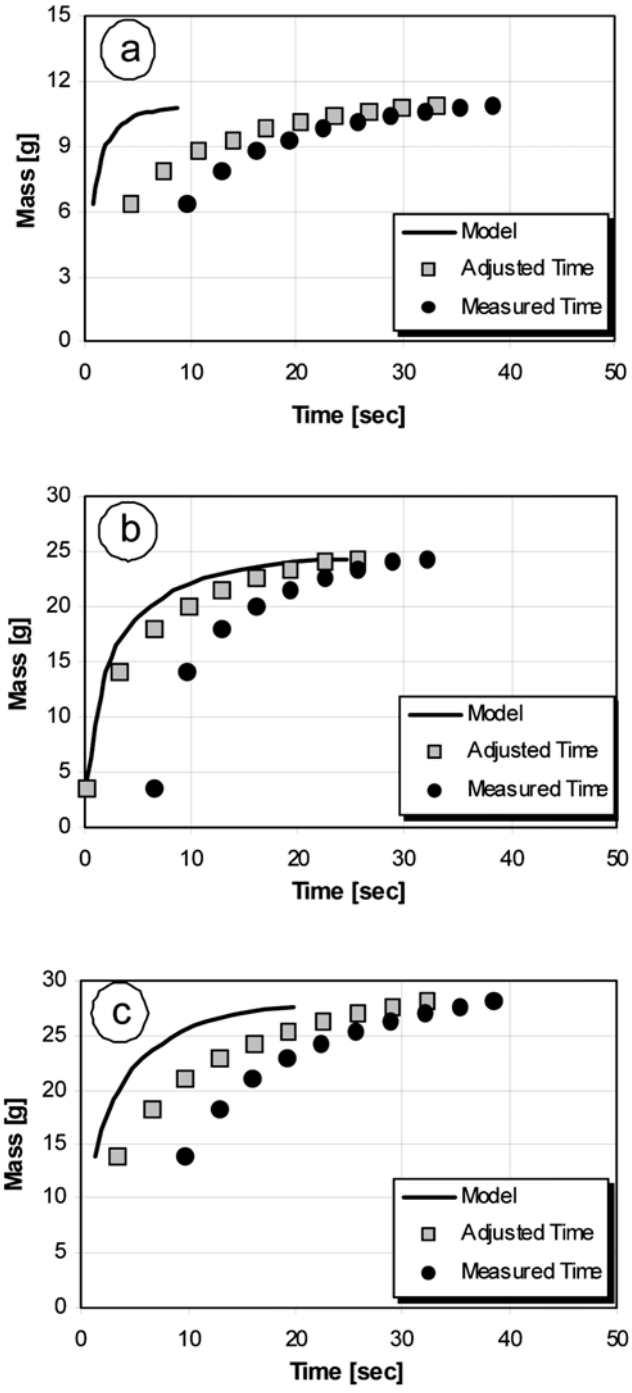

Figure 4. Imbibition of (a) n-hexane, (b) pure water, and (c) salt (5 molal $NaNO_3$) solution into air-dry 20/30 grade sand. Measured falling head K_S values are used in the Green and Ampt model, requiring the model to optimize only h_f and t_0.

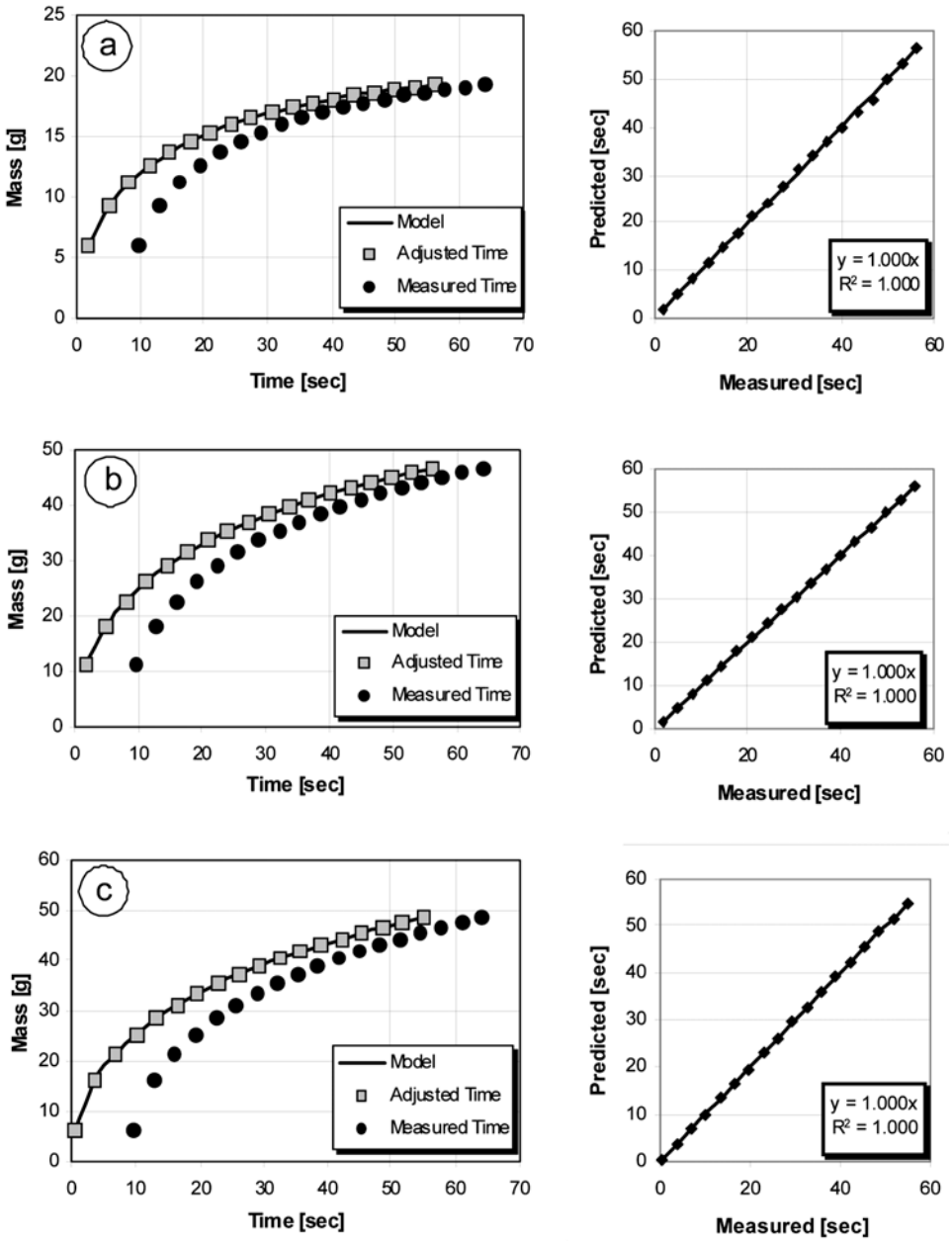

Figure 5. A comparison between predicted and measured imbibition of (a) n-hexane, (b) pure water, and (c) 5 molal $NaNO_3$ solution into air-dried 40/50 grade sand.

for the initially dry sands. In the revised (secondary) optimization procedure, t_0, θ_{FS}, and h_f in equation (8) were optimized and K_{FS} was simply updated in the process according to equation (9).

3. Results and Discussion

3.1. Hydraulic Conductivity

[19] The values of K_{FS} calculated from the optimized values of θ_{FS} to fit the Green and Ampt imbibition model were 1.5 to 20.7 times lower than the K_S values determined independently [*Klute and Dirksen*, 1986; *Wilson et al.*, 2000] (Table 3), with the greatest discrepancies observed in the coarsest materials and for the imbibition of n-hexane. The coarse sand results were expected, since wetting with upward imbibition leaves the largest pores filled with air, resulting in lower hydraulic conductivity than would be obtained for fully liquid saturated conditions [*Klute and Dirksen*, 1986]. In the case of n-hexane, a smaller contact angle gives rise to greater film flow and, therefore, to lower liquid saturation, as was noted for water imbibition into water-wet sand.

[20] The K_S values found in the falling head experiments would be expected to be applicable if the media were fully saturated behind the wetting front, leaving only the parameters h_f and t_0 to be optimized (Figures 3a–3c and 4a–4c). However, poor fit was obtained using measured K_S values versus using K_{FS} values that were determined from optimized values of θ_{FS} using equation (10). This result supports the conclusion that the actual hydraulic conductivity at the wetting front during imbibition is indeed lower than the fully saturated hydraulic conductivity of the sands. The fit

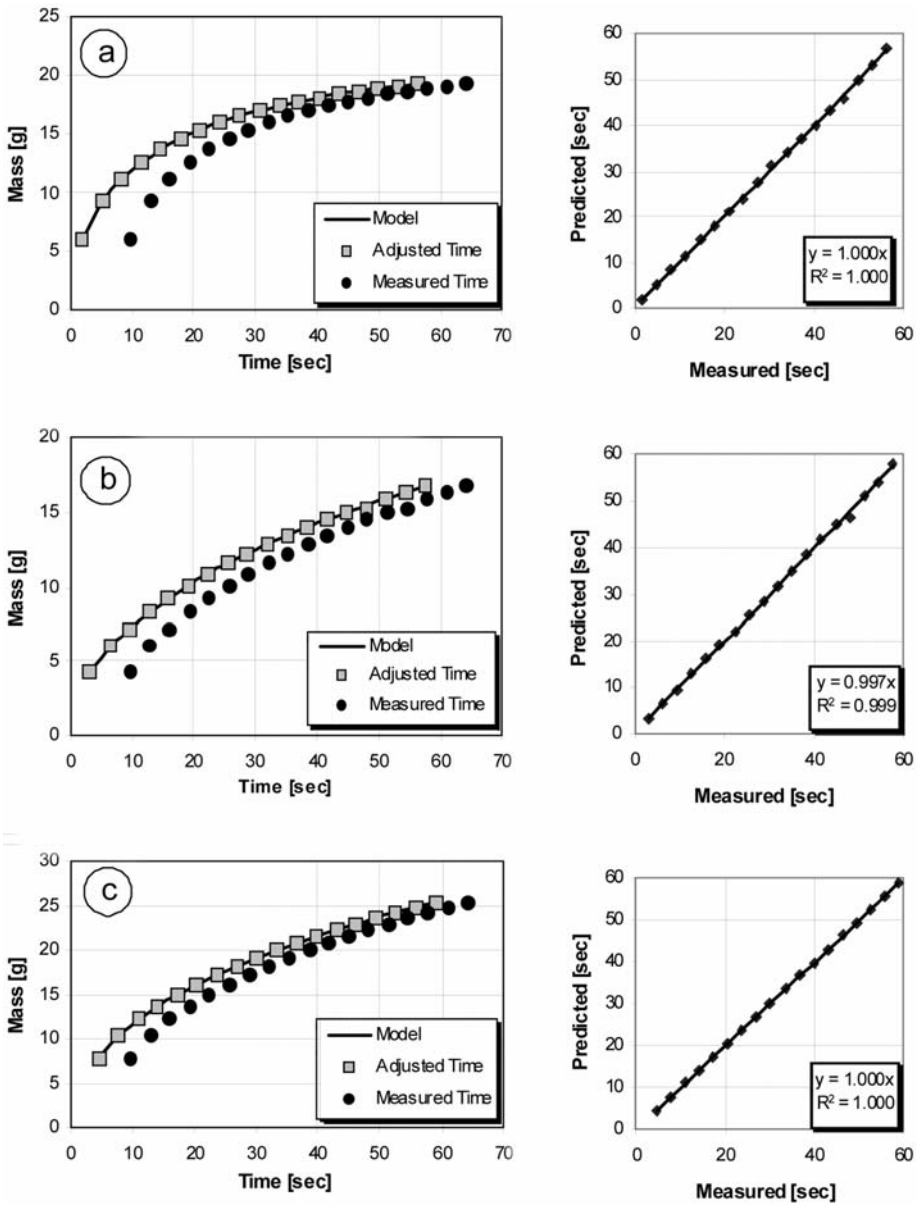

Figure 6. A comparison between predicted and measured imbibition of (a) n-hexane, (b) pure water, and (c) 5 molal $NaNO_3$ solution into prewetted 40/50 grade sand.

between the model and the adjusted data, as illustrated for the 40/50 grade sand, was excellent ($R^2 > 0.996$) when θ_{FS} was fitted and K_{FS} was updated according to equation (9), and far superior to the results obtained using measured values of K_s and n (Figures 5 and 6). The differences between K_S and K_{FS} were more significant for the two coarser sand grades (Table 3). The computed liquid content behind the wetting front θ_{FS} was between 0.211 and 0.300 for the four grades of Accusand®, whereas the measured porosities ranged from 0.324 to 0.337 (Table 2).

3.2. Static Method Versus Dynamic Method

[21] For the dynamic method, DCAs were calculated from the fitted values of h_d obtained from equation (8), and using equation (5) with h_d substituted for h_s. Our experimental results (Tables 4–7) suggest that dynamic DCAs can deviate significantly from their static values, which is consistent with observations in previous studies [e.g., *Blake*, 1993; *Siebold et al.*, 2000]. Computed DCAs were in accordance with expectations for definitions of static and dynamic DCAs, with the static values being about half those of the dynamic ones (Tables 4 and 5). The similarity between the DCAs for pure water and saline solution in dry sand (particularly in the static method results), despite their different surface tensions, is notable. A smaller effective pore radius (i.e., lower capillarity or greater contact angle) was computed using the dynamic method, relative to the static method, for all sand grades, even though the computed values of r for the two methods were very similar.

3.3. Dry Sand Versus Prewetted Sand

[22] Since it is rare to find soils that are completely dry (except near ground surface in arid environments), the air-dried sand results are of limited applicability. Therefore,

Table 4. Static Method Results for Dry Sand[a]

Sand	Solution	Capillary Rise, h_s[b] (cm)	Pore Radius, r[c] (cm)	Contact Angle (deg)
40/50	n-hexane	6.68 (0.10)	0.009 (0.0001)	0
	pure water	16.20 (0.25)	0.009 (0.0001)	23 (1.15)
	$NaNO_3$	14.17 (0.03)	0.009 (0.0001)	23 (1.71)
30/40	n-hexane	5.15 (0.10)	0.011 (0.0002)	0
	pure water	11.48 (0.19)	0.011 (0.0002)	32 (1.71)
	$NaNO_3$	10.04 (0.01)	0.011 (0.0002)	33 (1.59)
20/30	n-hexane	3.68 (0.07)	0.016 (0.0003)	0
	pure water	8.22 (0.03)	0.016 (0.0003)	32 (1.37)
	$NaNO_3$	7.13 (0.04)	0.016 (0.0003)	33 (1.22)
12/20	n-hexane	2.52 (0.09)	0.023 (0.0008)	0
	pure water	5.72 (0.10)	0.023 (0.0008)	30 (1.65)
	$NaNO_3$	4.99 (0.11)	0.023 (0.0008)	31 (1.26)

[a]Average values are shown from three repetitions conducted with each of the three test solutions (pure water, n-hexane, and 5 molal $NaNO_3$) imbibing into each of the four sand grades. The standard deviation of the three repetitions is shown in parentheses.
[b]Value of h_s was calculated from equation (6).
[c]Effective radius was calculated from equation (5) using results for n-hexane.

comparing DCAs developed in air-dried sand to those in prewetted sand is also of interest. The dynamic model was able to fit the data for both dry sand and prewetted sand quite well with plots of predicted versus measured time having $0.99 < \text{slope} < 1.01$ and $r^2 > 0.985$ (Figures 5 and 6). The DCAs obtained from the static method were essentially identical for pure and saline solutions, near 45° (Table 6), while the dynamic method showed much lower and differing DCAs for the two solutions (Table 7).

[23] *Weisbrod et al.* [2002] studied finger flow in air-dried versus prewetted Accusand® with both pure water and 5 molal $NaNO_3$. In those experiments, involving a dynamic wetting process, the two solutions migrated similarly in the air-dried sand while significant differences were observed in the prewetted sand. The degree of saturation at the tip of the fingers never exceeded 27% in the prewetted sand, while it was about 80 to 90% when the same infiltration conditions were used in air-dried sand. Limited work has been published on fingered flow in wetted media, and the effect of initial water content on finger development is not yet fully understood [*de Rooij*, 2000]. It is usually assumed, however, that a wetting fluid imbibing into liquid-coated porous media leads to a contact angle close to 0°, assuming that the imbibing fluid will freely wet the water-coated particle surfaces. These assumptions were confirmed here with the experimental results for dynamic wetting (Table 7).

Table 6. Static Method Results for Prewetted 40/50 Sand[a]

Solution	Capillary Rise, h_s[b] (cm)	Pore Radius, r[c] (mm)	Contact Angle[d] (deg)
Pure water	12.50 (0.16)	0.009 (0.0001)	45 (1.01)
5 molal $NaNO_3$	10.81 (0.13)	0.009 (0.0001)	46 (1.35)

[a]Each value represents three replications, with the standard deviation indicated in parentheses.
[b]Height of capillary rise calculated using equation (6).
[c]Effective pore radius representing the sand calculated using equation (5).
[d]Advancing contact angle of the solution on the sand calculated using equation (5).

[24] A dynamic contact angle of 21° was obtained for the 5 molal $NaNO_3$ solution imbibing into water-wetted sand (Table 7). This value was greater than that obtained for pure water imbibing into water-wetted sand and, as expected, lower than that obtained for imbibition into initially dry sand. These experimental results suggest that for the case of our prewetted sands, equation (3) should be rewritten as

$$\sigma_{sg_{water}} + \sigma_{sl} = \sigma_{sl} + \sigma_{lg_{saline}} \cos\gamma \tag{11}$$

where the solid-gas interface is now coated with a water film, and we have two interfacial forces, σ_{sl}, opposing one another,

Table 5. Dynamic Method Results for Dry Sand[a]

Solution	Pressure Potential, h_f[b] (cm)	Pore Radius, r[c] (cm)	K_{FS}[d] (cm/s)	Contact Angle[e] (deg)	Water Content, θ_{fs}[f]
		40/50			
n-hexane	7.71 (0.09)	0.007 (0.000)	0.058 (0.002)	0	0.267 (0.002)
Pure water	13.27 (0.95)	0.007 (0.000)	0.043 (0.004)	49 (3.5)	0.308 (0.009)
$NaNO_3$	13.38 (0.55)	0.007 (0.000)	0.031 (0.002)	41 (2.7)	0.282 (0.006)
		30/40			
n-hexane	6.55 (0.42)	0.009 (0.001)	0.068 (0.006)	0	0.235 (0.005)
Pure water	8.62 (0.04)	0.009 (0.001)	0.071 (0.002)	60 (0.14)	0.301 (0.003)
$NaNO_3$	9.36 (0.67)	0.009 (0.001)	0.047 (0.004)	52 (3.2)	0.269 (0.008)
		20/30			
n-hexane	6.01 (0.25)	0.010 (0.000)	0.063 (0.007)	0	0.189 (0.006)
Pure water	6.43 (0.56)	0.010 (0.000)	0.107 (0.015)	66 (2.2)	0.278 (0.001)
$NaNO_3$	6.41 (0.39)	0.010 (0.000)	0.074 (0.007)	63 (1.8)	0.252 (0.007)
		12/20			
n-hexane	4.85 (0.39)	0.012 (0.001)	0.049 (0.006)	0	0.147 (0.005)
Pure water	5.52 (0.49)	0.012 (0.001)	0.102 (0.032)	64 (2.4)	0.223 (0.006)
$NaNO_3$	4.57 (0.44)	0.012 (0.001)	0.116 (0.037)	66 (2.4)	0.222 (0.001)

[a]Average values are shown from three repetitions conducted with each of the three test solutions (pure water, n-hexane, and 5 molal $NaNO_3$) imbibing into each of the four sand grades. The standard deviation of the three repetitions is shown in parentheses.
[b]Capillary pressure potential fitted by the modified Green and Ampt model.
[c]Calculated from equation (5).
[d]As fitted by the modified Green and Ampt solution.
[e]Advancing contact angle of the solution on the sand calculated using equation (10).
[f]Water content θ_{fs} for K_{FS} fitted by the modified Green and Ampt solution.

Table 7. Dynamic Method Results for Prewetted 40/50 Sand[a]

Solution	Pressure Potential, h_f[b] (cm)	Pore Radius, r[c] (cm)	K_{FS}[d] (cm/s)	Contact Angle[e] (deg)	Water Content, θ_{FS}[f]
Pure water	20.27 (0.02)	0.007 (0.000)	0.006 (0.001)	2 (0.96)	0.141 (0.007)
5 molal $NaNO_3$	16.62 (0.13)	0.007 (0.000)	0.006 (0.002)	21 (1.10)	0.141 (0.020)

[a]Each value represents three replications, with the standard deviation indicated in parentheses.
[b]Capillary pressure potential fitted by the modified Green and Ampt model.
[c]Effective pore radius calculated using the solution-specific parameters (σ_{lg} and ρ_l) for n-hexane, as well as that optimized by the modified Green and Ampt model (h_f) while assuming γ to be zero for n-hexane (imbibition into air-dried porous media only).
[d]K_{FS} fitted by the modified Green and Ampt model.
[e]Advancing contact angle of the solution on the sand calculated via equation (12) using fitted parameters.
[f]Degree of saturation θ_{fs} for K_{FS} fitted by the modified Green and Ampt model.

due to the water-wetted solid surface of the sand grains. Equation (11) may be rearranged to yield

$$\gamma = \cos^{-1}\left(\frac{\sigma_{\mathrm{lg}_{water}}}{\sigma_{\mathrm{lg}_{saline}}}\right) \tag{12}$$

which predicts a contact angle of 0° for water and 25° for saline solution, consistent with our experimental results (Table 7). For imbibition of saline solutions into water-wetted porous media, equations (12), (5), and (8) can be combined to yield explicit relations between the wetting front pressure, the effective pore radius, and the dynamic contact angle.

[25] The assumption of a fully saturated wetting front used to interpret the static results appears to be even less applicable to prewetted sand than to air-dried sand. The apparent height of capillary rise h was lower in the prewetted sand, and the DCA was in fact higher (Tables 4 and 6), which is likely due to the use of measured porosities for the water content behind the wetting front in the static case. Using these assumptions in interpreting the dynamic imbibition data resulted in significant errors in calculated contact angles (Table 7).

4. Summary and Conclusions

[26] Static and dynamic methods were employed to determine apparent DCAs for solutions of different surface tensions on four silica sands. The results obtained using the two methods differed significantly. The static method did not include sufficient data to estimate DCA and effective saturation simultaneously. In the static tests, the height of the liquid rise in the porous media was computed from the mass of water imbibed and the assumed (saturated) water content behind the wetting front. With no other data available, it was not possible to independently estimate the actual liquid content behind the wetting front. In prewetted sands, this led to estimates of the apparent DCA that were at odds with the expected 0° DCA for imbibition of pure water into water-wet sand.

[27] In contrast, the dynamic method for analysis of imbibition into water-wet sand yielded a DCA of 2° for water and 21° for 5 molal $NaNO_3$, in excellent agreement with the values of 0° and 25° calculated using Young's equation. The dynamic method employed a Green and Ampt–type model that captured the effects of incomplete saturation using the retention and hydraulic conductivity model of *Brooks and Corey* [1964] to calculate the effective degree of saturation. The estimated DCAs in the static and dynamic methods were compared for dry sand, and showed that the DCAs computed using the dynamic method were higher than those computed using the static method for both pure water and 5 molal $NaNO_3$ imbibition.

[28] Using independently measured hydraulic conductivity K_S as a fixed parameter in the Green and Ampt imbibition model left only two parameters (h_f and t_0) to be fitted. With this constraint, the model did not fit the data well. The degree of saturation of the porous media in the dynamic tests, calculated using the *Brooks and Corey* [1964] relationship, suggested hydraulic conductivity values 1.5 to 20.7 times lower than independently measured values of K_S. When these values were employed, the model fit the data exceptionally well (e.g., $R^2 > 0.99$).

[29] The data obtained in this study strongly support the contention that the assumption of 0° DCA is not valid for imbibition into clean dry silica sand, or for imbibition of solutions with high surface tension into porous media wetted with lower surface tension liquids. To the best of our knowledge, these experimental results provide the first observations of a DCA effect (nonzero contact angle) between two miscible fluids.

[30] **Acknowledgments.** We would like to thank Maria Dragila for many constructive discussions during the experimental stages. The authors are also greatly indebted to the four anonymous reviewers whose comments significantly improved this manuscript. This work was funded by the Department of Energy under contract DE-FG07-98ER14925 and had the support of the Oregon Agricultural Experiment Station.

References

Bachmann, J., S. K. Woche, M.-O. Goebel, M. B. Kirkham, and R. Horton (2003), Extended methodology for determining wetting properties of porous media, *Water Resour. Res.*, *39*(12), 1353, doi:10.1029/2003WR002143.

Blake, T. D. (1993), Dynamic contact angles and wetting kinetics, in *Wettability*, edited by J. C. Berg, pp. 49–50, Marcel Dekker, New York.

Brooks, R. H., and A. T. Corey (1964), Hydraulic properties of porous media, *Hydrol. Pap. 3*, Colo. State Univ., Ft. Collins, Colo.

Burdine, N. T. (1953), Relative permeability calculations from pore-size distribution data, *Trans. Am. Inst. Min. Metall. Pet. Eng.*, *198*, 71–77.

Clarke, A., T. D. Blake, K. Carruthers, and A. Woodward (2002), Spreading and imbibition of liquid droplets on porous surfaces, *Langmuir*, *18*, 2980–2984, doi:10.1021/la0117810.

Daniel, R. C., and J. C. Berg (2006), Spreading on and penetration into thin, permeable print media: Application to ink-jet printing, *Adv. Colloid Interface Sci.*, *123–126*, 439–469, doi:10.1016/j.cis.2006.05.012.

Denesuk, M., G. L. Smith, B. J. J. Zelinski, N. J. Kreidl, and D. R. Uhlmann (1993), Capillary penetration of liquid droplets into porous materials, *J. Colloid Interface Sci.*, *158*, 114–120, doi:10.1006/jcis.1993.1235.

de Rooij, G. H. (2000), Modeling finger flow of water in soils owing to wetting front instability a review, *J. Hydrol.*, *231–232*, 277–294, doi:10.1016/S0022-1694(00)00201-8.

Grand Junction Projects Office (1996), Vadose zone characterization project at the Hanford Tank Farms, U.S. Dep. of Energy, Grand Junction, Colo.

Green, W. H., and G. A. Ampt (1911), Studies on soil physics: I. Flow of air and water through soils, *J. Agric. Sci.*, *4*, 1–24, doi:10.1017/S0021859600001441.

Hilpert, M., and A. Ben-David (2009), Infiltration of liquid droplets into porous media: Effects of dynamic contact angle and contact angle hysteresis, *Int. J. Multiphase Flow*, *35*(3), 205–218, doi:10.1016/j.ijmultiphaseflow.2008.11.007.

Holman, R. K., M. J. Cima, S. A. Uhland, and E. Sachs (2002), Spreading and infiltration of inkjet-printed polymer solution droplets on a porous substrate, *J. Colloid Interface Sci.*, *249*, 432–440, doi:10.1006/jcis.2002.8225.

Klute, A., and C. Dirksen (1986), Hydraulic conductivity and diffusivity: Laboratory method, in *Methods of Soil Analysis, Part 1*, *Soil Sci. Soc. Am. Book Ser.*, vol. 5, edited by A. Klute, pp. 687–734, Soil Sci. Soc. of Am., Madison, Wis.

Malik, R. S., S. Kumar, and I. S. Dahiya (1984), An approach to quick determination of some water transmission characteristics of porous media, *Soil Sci.*, *137*, 395–400, doi:10.1097/00010694-198406000-00003.

McBride, J. F., C. S. Simmons, and J. W. Cary (1992), Interfacial spreading effects on one-dimensional organic liquid imbibition in water-wetted porous media, *J. Contam. Hydrol.*, *11*, 1–25, doi:10.1016/0169-7722(92)90031-9.

Meyers, D. (1991), *Surfaces, Interfaces, and Colloids: Principles and Applications*, VCH, New York.

Schroth, M. H., S. J. Ahearn, J. S. Selker, and J. D. Istok (1996), Characterization of Miller-similar silica sands for laboratory hydrologic studies, *Soil Sci. Soc. Am. J.*, *60*(5), 1331–1339.

Selker, J. S., and M. H. Schroth (1998), Evaluation of hydrodynamic scaling in porous media using finger dimensions, *Water Resour. Res.*, *34*, 1935–1940, doi:10.1029/98WR00625.

Selker, J. S., C. K. Keller, and J. T. McCord (1999), *Vadose Zone Processes*, CRC Press, Boca Raton, Fla.

Siebold, A., M. Nardin, J. Schultz, A. Walliser, and M. Oppliger (2000), Effect of dynamic contact angle on capillary rise, phenomena, *Colloids Surf. A*, *161*, 81–87, doi:10.1016/S0927-7757(99)00327-1.

Weisbrod, N., M. R. Niemet, and J. S. Selker (2002), Imbibition of saline solutions into dry and prewetted porous media, *Adv. Water Resour.*, *25*, 841–855, doi:10.1016/S0309-1708(02)00038-6.

Weisbrod, N., M. R. Niemet, T. McGinnis, and J. S. Selker (2003), Water vapor transport in the vicinity of imbibing saline plumes: Homogeneous and layered unsaturated porous media, *Water Resour. Res.*, *39*(6), 1145, doi:10.1029/2002WR001539.

Weisbrod, N., M. R. Niemet, M. L. Rockhold, T. McGinnis, and J. S. Selker (2004), Migration of saline solutions into variably saturated porous media, *J. Contam. Hydrol.*, *72*, 109–133, doi:10.1016/j.jconhyd.2003.10.013.

Wilson, M. A., W. D. Hoff, J. E. Brown, and M. A. Carter (2000), A falling head permeameter for the measurement of the hydraulic conductivity of granular solids, *Rev. Sci. Instrum.*, *71*, 3942–3946, doi:10.1063/1.1310349.

Zadrazil, A., F. Stepanek, and O. K. Matar (2006), Droplet spreading imbibition and solidification on porous media, *J. Fluid Mech.*, *562*, 1–33, doi:10.1017/S0022112006000875.

T. McGinnis and J. S. Selker, Department of Biological and Ecological Engineering, Oregon State University, Corvallis, OR 97331, USA. (selkerj@engr.orst.edu)

M. R. Niemet, CH2M HILL, Corvallis, OR 97330, USA. (michael.niemet@ch2m.com)

M. L. Rockhold, Pacific Northwest National Laboratory, Richland, WA 99352, USA. (mark.rockhold@pnl.gov)

N. Weisbrod, Department of Environmental Hydrology and Microbiology, Ben-Gurion University, Midreshet Ben-Gurion, 84990, Israel. (weisbrod@bgu.ac.il)